Michigan State University

National Superconducting Cyclotron Laboratory

SHELL MODEL: CHAOS, COMPLEXITY, THERMALIZATION

Invited talk presented at the Workshop on Parity and Time Reversal Violation in Compound Nuclear States and Related Topics, Trento, Italy, October 1995

VLADIMIR ZELEVINSKY, B. ALEX BROWN, and MIHAI HOROI

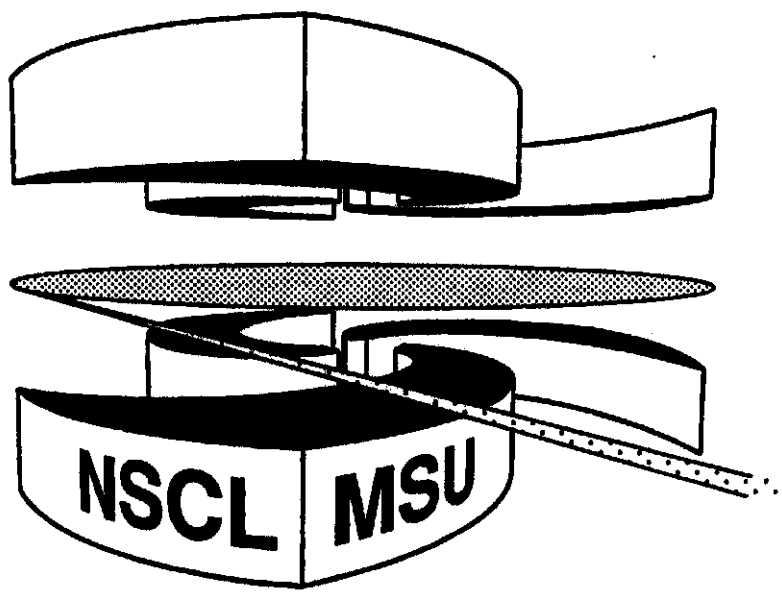

MSUCL-1025 **APRIL 1996**

SHELL MODEL: CHAOS, COMPLEXITY, THERMALIZATION

Vladimir ZELEVINSKY, B. Alex BROWN
Department of Physics and Astronomy and
National Superconducting Cyclotron Laboratory,
East Laming, MI 48824 USA

Mihai HOROI
Physics Department, Central Michigan University,
Mount Pleasant, MI 48859 VS.4

The nuclear shell model is analysed as a generic example of a many-fermion quantum system with strong interaction. The exact solution of the eigenvalue problem with a realistic residual interaction in truncated Hilbert space gives the energy spectrum and eigenstates which are the complicated superpositions of basic configurations projected onto good angular momentum and isospin. Although the energy spectra reveal the standard signatures of quantum chaos jn local level statistics, they do not reflect the evolution of complexity along the spectrum. The complexity and similarity of individual states are studied by means of information entropy in the shell model basis. The interrelation between quantum chaos, Fermi liquid theory and thermalisation is discussed.

1 Introduction

Although the number of publications devoted to quantum chaos increases exponentially, see for example [1,2,3,4,5,6,7,8] and references therein, with the rate which exceeds tbe rate for the entire volume of scientific publications by a factor 4, one of the main physical questions remains unanswered: What is the role of chaotic dynamics in actual many-body quantum systems with strong interaction between the constituents?

We will not discuss hem the formal problems of the rigorous definition of quantum chaos. We just mention in this connection that, contrary to the widely accepted viewpoint that quantum chaos exists only as a shadow of classical chaoticity, the situation seems to be opposite: classical chaos is a transient phenomenon specific for the short wavelength limit. After some time which in reality can be very long, quantum spreading prevails over the divergence of semiclassical trajectories. However this theoretical statement does not facilitate the real problem of addressing the physical question of the preceding paragraph. It can be done only by the analysis of specific realistic systems.

Such an analyst frequently has two limitations. First, it is carried out for the simplest systems with a small number of degrees of freedom. The

prototypical case is a quantum billiard where "one-body chaos" is generated by the shape of the potential. Second, the analysis often stops at the level statistics assuming that the Wigner nearest level spacing distribution and/or the spectral rigidity display generic signatures of quantum chaos. The first limitation eliminates such an important source of chaotic dynamics as particle interaction which distinguishes realistic "many-body chaos" [9]. The second limitation deliberately excludes from the consideration the evolution of chaotic signatures along the spectrum which is hidden in the structure of generic wave functions.

Our approach [10,11,12] has a primary goal to overcome these limitations. Atomic nuclei present an appropriate object for such studies by the multitude of reasons:

- the nucleus is a strongly interacting Fermi system;
- nuclear spectroscopy shows onset of chaos in the local level statistics at relatively low excitation energy of 3-5 MeV [13,14,15];
- Bohr's picture of compound states [16] which is the base of all statistical approaches to nuclear phenomena strongly resembles the notion of quantum chaos;
- many experimental results as, for example, Porter-Thomas distribution of widths of neutron and proton resonances [1,2,3], enhancement of weak interactions [17], parity nonconservation in fission [18], spreading width of isobaric analog states [19,20], saturation of widths of giant resonances [21,22], narrowing of multiple giant excitations [23,24], fluctuations in rotational cascades [25,26] and so on, were interpreted in terms of chaotic dynamics;
- shell model calculations determine the semiempirical hamiltonians which work well in the region of available spectroscopic information [27] and can be extrapolated beyond this region;
- it is possible to satisfy the conservation laws and ensure that the eigenstates have correct exact quantum numbers;
- the corresponding dimensions, of the order 10^3, are sufficient for obtaining statistically reliable results, and, at the same time, are practical to be effectively and rapidly handled [28].

Encouraging studies have already been carried out using realistic models [29,30,31,32,33] and simplified schemes [34,35]. Similar work was performed for heavy atoms with dimensions of several hundreds [36].

2 Shell-model calculations

We base our analysis on the exact diagonalization of the effective semiempirical hamiltonian H in a large $N \times N$ Hilbert space spanned by a truncated set of shell-model configurations. Each configuration is characterized by the distribution ("partition") of independent fermions over available spherical single-particle orbitals. Within a configuration, various ways to occupy the magnetic substates of the j-levels give rise to the "m-scheme" Slater determinants.

The hamiltonian H keeps rotational and isospin invariance. The necessity of using the appropriate $J^\pi T$ states was demonstrated in the first studies of quantum chaos in the shell model [29]. The basis states $|k\rangle$ have good quantum numbers of the total angular momentum J, its projection M, parity π, isospin T and its projection T_3. Therefore they are far from being simple Slater determinants. This "premixing" is absent in the analysis of high spin rotational bands in the framework of the cranking model [26].

The effective shell-model hamiltonian H consists of the independent particle (one-body) part H_0 and the residual interaction H' of the two-body type. The unperturbed hamiltonian H_0 describes noninteracting fermions in the mean field of the appropriate spherical core. In the projected basis $|k\rangle$, the residual interaction H' has both diagonal and off-diagonal matrix elements. The diagonal part already lifts some degeneracy within a partition. Full diagonalization in each sector with given exact quantum numbers leads to the stationary states $|\alpha\rangle$,

$$H|\alpha\rangle = E_\alpha|\alpha\rangle, \tag{1}$$

which can be represented by superpositions of unperturbed states $|k\rangle$,

$$|\alpha\rangle = \sum_k C_k^\alpha |k\rangle. \tag{2}$$

The orthonormalized amplitudes C_k^α can be taken as real in the case of the interaction invariant under time reversal. A number N_α of significant components $|k\rangle$ characterizes the delocalization of a state $|\alpha\rangle$ in the given basis. The corresponding amplitudes have an order of magnitude $N_\alpha^{-1/2}$. A completely delocalized function would have N_α close to the space dimension. Direct estimates [17] show that the matrix elements of simple operators between such complicated states are suppressed $\sim N_\alpha^{-1/2}$ if the coefficients (2) are chaotic ("N-scaling"), the phase coherence is absent and only the weights $W_k^\alpha \sim N_\alpha^{-1}$ are important for the estimates. With the level density enhanced roughly by a factor N_α, this qualitatively explains enhancement of weak interactions and saturation of the spreading widths.

We will discuss mostly the results for a system of valence particles in one major shell, for example 12 particles in the *sd* shell (24 states including $0d_{5/2}$, $0d_{3/2}$ and $1s_{1/2}$) when the one-body part of the total hamiltonian is due to the core ^{16}O. This system mimics (for $T_3 = 0$) a subset of states in the ^{28}Si nucleus. We use the Wildenthal hamiltonian[27] obtained by fitting more than 400 binding energies and excitation energies for the *sd*-shell nuclei; for the recent comparison of experiment and theory in ^{28}Si see[37]. Similar studies were performed using the "proton-neutron" $(p-n)$ formalism with no explicit isospin where we used, along with the Wildenthal interaction rewritten for the $p-n$ scheme (WPN), the interaction (WPNC) which explicitly violates isospin on the experimentally allowed level[38]. All calculations were carried out with the computer program OXBASH[28], which uses the *m*-scheme basis states together with the projection operators to construct and diagonalize matrices with good J and T in the isospin formalism and good J in the $p-n$ formalism.

Taking into account J and T conservation, there are 63 non-vanishing two-body matrix elements $\langle (j_1 j_2)_{JT} | H' | (j_3 j_4)_{JT} \rangle$ in *sd*-shell space. Being in general of the order of an MeV, the two-body matrix elements are not random; for example they show pair correlations in the $T = 1$ states with even angular momenta. In our calculations, we mostly use the $J^\pi T = 2^+0$ and 0^+0 classes of states, with dimensions 3276 and 839, respectively.

The signatures of quantum chaos come exclusively from the particle interaction (H_0 is very simple and does not lead to one-body chaos). Some relevant properties of the hamiltonian can be noticed prior to actual diagonalization. Long ago such analyses were carried out by statistical spectroscopy[39].

Diagonal matrix elements are dominated by the one-body part H_0. The two-body diagonal contributions split the degenerate levels within the partitions so that each partition partly overlaps with the other partitions. In our $A = 28$ example, the diagonal part of the hamiltonian is spread from -120 MeV to -60 MeV. The basis states $|k\rangle$ will be mixed by the off-diagonal part H'. Due to the premixing related to J and T projection, the two-body matrix elements between the many-body basis states are reduced by an order of magnitude. as it should be according to the N-scaling[17]: the dimension of a partition is typically 10^2 and the reduction factor is $\sim N^{-1/2}$.

Without the full knowledge of the strength function, one can describe the fragmentation of simple states by its lowest moments[39]. The centroid $\bar{E}_k$ of the energy distribution of the basis state $|k\rangle$ coincides with the diagonal element H_{kk}. The spread of the unperturbed energies due to the diagonal elements of the interaction can be characterized by the rms deviation Δ_E of the centroids $\bar{E}_k$ from the energy center; for the 2^+0 states $\Delta_E \approx 8$ MeV. The

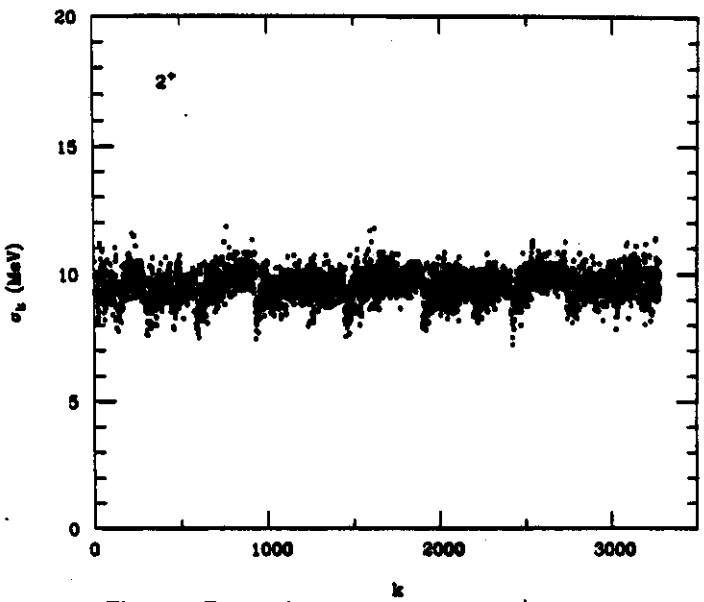

Figure 1: Energy dispersions σ_k of basis 2^+0 states

energy dispersion of basis states due to the off-diagonal interaction is

$$\sigma_k^2 \equiv \sum_\alpha (E_\alpha - \bar{E}_k)^2 W_k^\alpha = \sum_{l(\neq k)} (H'_{lk})^2. \tag{3}$$

The energy dispersion (3) of individual 2^+0 basis states turns out (Fig. 1) to be uniform, $\sigma_k \approx \bar{\sigma} \approx 10$ MeV over the entire space. The remnants of the partition structure are visible at the low edges of partitions. This might be caused by a random choice of the initial simple states in the projection procedure. The dispersion σ_k is closely related to the spreading width (in the "strong coupling" case[22,40] $\Gamma \simeq 2\bar{\sigma}$). The uniformity of the dispersion supports the idea of saturation[22] which has important consequences for damping of giant resonances.

Since variations of the effective spreading (3) of the basis states around the mean value $\bar{\sigma}$ are small, one can work out [41] a simple truncation method to reduce a huge shell-model hamiltonian matrix to a manageable size. The method was tested for the *sd* and *fp* shells and was proven to be very efficient. In the middle of the *fp* shell (JT dimensions of the order of a few million) the size of the matrix is effectively reduced to a few thousand.

The partition structure gives rise to distinct band-like features. As a rule,

the interaction between the states $|k\rangle$, which are widely separated in centroid energy $\bar{E}_k$, is weaker than between the close configurations. This interaction energy range can be measured using the definition [42]

$$\omega_k^2 = \frac{1}{\sigma_k^2} \sum_l (\bar{E}_k - \bar{E}_l)^2 |\tilde{H}_{kl}|^2. \tag{4}$$

The banded structure of the shell-model hamiltonian within the $J^\pi T$ class is the reflection of the selection rules specific for the two-body interaction. In contrast to the banded random matrices (BRM) [43,44,45] which have no regular diagonal structure or the closer two-body random ensemble [3,35], our hamiltonian matrix is neither random nor banded in the strict meaning of this term because it is impossible to reach a precisely banded form by reordering. The effective width of the band is $\omega \approx 7.5$ MeV both for 0^+0 and 2^+0 states. This corresponds to $b \approx 200$ to 250 unperturbed states within the band. The parameter b^2/N is therefore very large in our case which implies that the localization properties of the eigenstates are different from those considered in [45].

The primary characteristic of the spectrum is the level density

$$\rho(E) = \sum_\alpha \delta(E - E_\alpha). \tag{5}$$

It is normalized to the total number of states, $\int dE \rho(E) = N$. The total dispersion of energy

$$\sigma_E^2 \equiv \frac{1}{N} \int dE (E - \bar{E})^2 \rho(E) = \bar{\sigma}^2 + \Delta_E^2 \tag{6}$$

consists of (added in quadratures) the spread of centroids defined by the diagonal part of the hamiltonian and the fragmentation width (3) due to the off-diagonal part. With the above-mentioned values of $\bar{\sigma}$ and Δ_E for the 2^+0 states we get $\sigma_E = 13$ MeV.

The random matrix theory usually considers matrix elements of the hamiltonian as random normally distributed variables. Canonical Gaussian ensembles with no regularly increasing diagonal elements have nothing to do with the evolution along the spectrum ("secular" behavior) and can properly account for the local correlations and fluctuations only. Moreover, the actual distribution of off-diagonal matrix elements in the "natural" shell model basis is quite different from Gaussian. The analysis [36] of the similar problem for a heavy atom showed that the actual distribution can be written in the form analogous to the Porter-Thomas distribution,

$$P_\kappa(\tilde{H}_{kl}) = \frac{1}{2}[(2\tilde{H})^{\kappa+1}\Gamma(\kappa+1)]^{-1} |\tilde{H}_{kl}|^\kappa e^{-|\tilde{H}_{kl}|/2\tilde{H}} \tag{7}$$

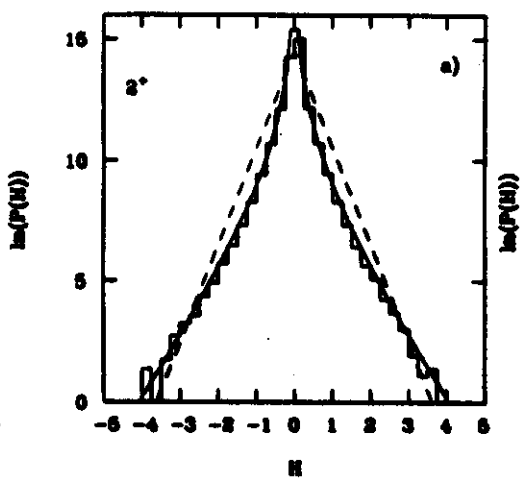

Figure 2: The distribution of off-diagonal matrix elements (in MeV) between the 2^+0 states (histogram), dashed line - pure exponential fit, eq.(7) with $\kappa = 0$, solid line - fit with $\kappa = -2$.

where Γ stands for the Γ-function and κ is a numerical parameter. The distribution of matrix elements found in the shell-model calculations [46] and in the interacting boson model [47] also agree with (7). Since our study reveals a very similar picture, the conclusion is plausible that this class of distributions is generic for the many-body interactions in heavy atoms or nuclei. For the distribution (7) taken literally for all values of $\tilde{H}_{kl}$, the mean absolute value of $\tilde{H}_{kl}$ is $2(\kappa+1)\tilde{H}$. The power κ found in [36] is close to the Porter-Thomas value -1/2.

The Porter-Thomas distribution for the reduced widths γ of the resonances follows from the Gaussian distribution for the decay amplitudes A if the proportionality $\gamma \propto |A|^2$ is assumed. Therefore eq.(7) implies that the normally distributed quantities in the realistic case are not the off-diagonal matrix elements themselves, as would be the case in Gaussian random matrix ensembles, but rather some quantities resembling square roots of them. The reason might be the domination of multipole-multipole forces. This is by construction the case in the interacting boson model. The Coulomb interaction in atoms is actually determined by a small number of low multipoles. The specific role of the pairing and quadrupole interactions in nuclei is also well known.

The distribution (7) diverges at small values of the matrix elements if $\kappa \leq -1$. In the actual analysis it is difficult to make a precise fit to this region. Fitting the rest of the histogram we allow all values of κ. The distribution function for 5.36×10^6 off-diagonal matrix elements between the 2^+0 states

is shown in Fig. 2. Except for the region around zero and extreme wings corresponding to the exceptionally big elements, the distribution is in good agreement with expression (7) for $\kappa = -2$. The fit covers a change of matrix elements by four orders of magnitude. The off-diagonal matrix elements for the 0^+0 states agree with the distribution (7) at $\kappa = -1$. The origin of the apparent difference in the preexponent factor for different classes of states is not clear at this point.

3 Level statistics

The total density $\rho(E)$ of states with given values of exact integrals of motion vanishes at boundaries of the finite spectrum, being maximum in the middle. The GOE predicts the Wigner semicircle rule for the level density. On the other hand, due to the two-body character of interaction there is a noticeable number of vanishing matrix elements in the truncated configuration space, and all many-body matrix elements are determined by a small number of the two-body matrix elements. However the realistic interaction is not strong enough to destroy completely the partition structure. In such cases, we should expect the level density $\rho(E)$ to be closer to the Gaussian shape [3]. The transition from Gaussian to semicircle level density occurs [48,3] when many-body forces are introduced, lifting the selection rules for interactions between the partitions. The two-body matrix elements are the same for all classes of states with various J and T which can induce the correlations between the classes.

Depicting the level densities for 0^+0 and 2^+0 states as histograms we can fit both of them, Fig. 3, by the Gaussians with the same values of the centroid $E_0 = -90$ MeV and the dispersion $\sigma_E = 13$ MeV predicted above. The Gaussian shape of the level density, with the smaller dispersion $\Delta_E \approx 8$ MeV, is formed entirely due to the combinatorial nature of the fermionic excitation spectrum already for the unperturbed energies H_{kk} with no off-diagonal interaction. In the $p-n$ formalism, we get practically the same results for the level density of the superpositions of the states with different (all) isospins. The different isospin sectors have similar properties defined by a common two-body interaction.

We can also generate the random matrix ensemble defined by the actual exponential distribution of the matrix elements (7). Then the many-body matrix elements are uncorrelated, and the level density agrees with the semicircle law. The difference between the empirical Gaussian level density and the semicircle should be ascribed to the correlations within the many-body hamiltonian determined by a small number of two-body matrix elements regardless of their regularity or randomness. The initial part of the spectrum agrees also with the

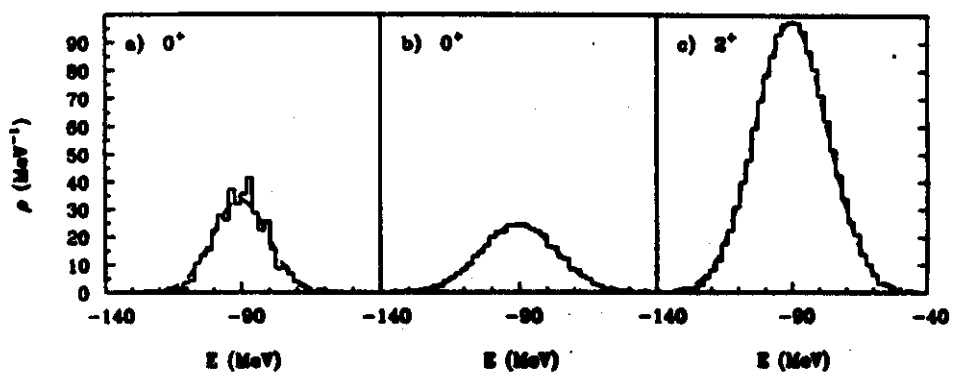

Figure 3: Level densities for the 0^+0 with no off-diagonal interaction (panel *a*) and for the 0^+0 and 2^+0 states with the realistic hamiltonian, panels *b* and *c*, respectively. The results of calculations are shown by the histograms and Gaussian fits by the dashed lines.

Fermi-gas level density[2] but at high excitation energy the Fermi-gas approach breaks down due to limitations of the finite Hilbert space.

The degeneracies caused by the shell structure in the spherical mean field are lifted by the residual interaction. In the stochastic limit, the mixing by the off-diagonal hamiltonian leads to the level repulsion and to a more uniform level spacing distribution. It results in the nearest level spacing distribution close to the Wigner surmise

$$P_W(s) = \frac{\pi}{2} s e^{-(\pi/4)s^2}. \tag{8}$$

The linear repulsion and Gaussian tail are the distinctive features of chaotic level statistics in contrast to the Poisson distribution of random events $P_P(s) = e^{-s}$ characteristic for integrable systems. Here $s = (E_{\alpha+1} - E_\alpha)/\bar{D} \equiv \mathcal{E}_{\alpha+1} - \mathcal{E}_\alpha$ is the nearest neighbor spacing in units of the local average spacing $\bar{D}$. This rescaling, or unfolding[3], $E_\alpha \rightarrow \mathcal{E}_\alpha$, is important to separate local level correlations from the global secular behavior.

Fig. 4 shows the nearest level spacing distribution $P(s)$ for 0^+0 states and the variable residual interaction. The relative intensity of the off-diagonal matrix elements is equal to $\lambda = 0.0, 0.1$ and 0.2, respectively. The noninteracting case reveals the Poisson-like distribution. The transition to the Wigner distribution occurs at $\lambda \approx 0.2$ of the realistic value, when typical off-diagonal matrix elements are of the order of the mean level spacing. The level spacing

distribution is universal as can be seen for the other $J^\pi T$ classes. An analysis shows that the interpartition interaction is responsible for establishing the Wigner level spacing distribution. Diagonalization within the single largest partition alone both for 0^+0 and for 2^+0 states, results in a distribution with an excess of small and large spacings. Qualitative features of the Wigner distribution appear after the diagonalization is performed in the model space of the three largest partitions. The $p-n$ formalism reveals the intermediate level spacing distribution due to the absence of mixing and repulsion between levels of different isospin. It is known that a superposition of many independent level sequences leads to the Poisson limit[49].

An interesting theoretical problem is related to the precise form of the level repulsion at small distances s. The GOE and regular dynamics predict the behavior $P(s) \propto s^\beta, \quad s \to 0$, with $\beta = 1$ and $\beta = 0$, respectively. There is no consistent theory explaining how the Poisson level spacing evolves into the Wigner distribution as the stochastization occurs and levels repel each other. Various scenarios include (i) a decreasing finite value of $P(s = 0)$ determined[50] by the regular and chaotic volume fractions of the classical phase space (the similar change was found[51,52] if the decay channels are open and the levels acquire the finite lifetime); (ii) the fractional power law $P(s) \sim s^\beta, \quad 0 < \beta < 1$ [53], used with variable success in interpolation formulae[3,7] (the correlation of β with the localization of wave functions was pointed out in [7]); (iii) the linear repulsion in a narrow region of spacings comparable to the magnitude of perturbation as implied by perturbation theory; (iv) the logarithmic singularities $\sim \ln(1/s)$ due to the presence of strictly forbidden [54] or exponentially small[55] matrix elements. The perturbative arguments do not take into account the abundance of small off-diagonal matrix elements which seems to be a generic feature of realistic systems. In the semiclassical domain it can occur if the classical phase space consists of separated parts. The degeneracy of the states localized in different areas would lead to the Poisson distribution of level spacings. However the quantum tunneling restores the communication between those areas. To study the region of $s \ll 1$ with high precision, one needs much better statistics. It can be achieved combining properly the data for different classes of states and for the variable interaction strength.

It is known[3,56,57] that chaotic dynamics lead to rather rigid spectra. The level repulsion creates a sequence of levels which "crystallize"; the fluctuations are suppressed in comparison with a pure random sequence. As an appropriate quantitative measure, the spectral rigidity $\Delta(L)$ is used,

$$\Delta(L) = \langle \min_{A,B} \int_x^{x+L} \frac{d\mathcal{E}}{L} [\mathcal{N}(\mathcal{E}) - A\mathcal{E} - B]^2 \rangle_x. \qquad (9)$$

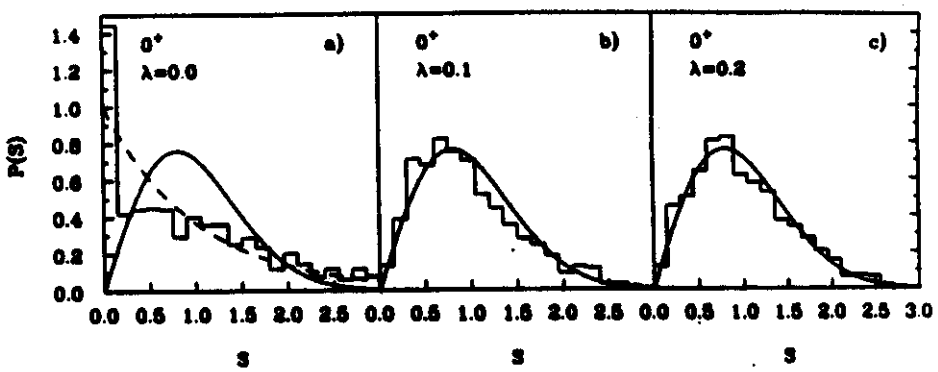

Figure 4: Nearest level spacing distribution (histograms) compared to the Wigner surmise (solid lines) and the Poisson distribution for the 0^+0 states at different interaction strength, $\lambda = 0$, 0.1 and 0.2 (panels a,b and c, respectively).

Here the average is taken of integral deviations of the cumulative unfolded level number $\mathcal{N}(\mathcal{E})$ from the best linear fit over various (overlapped) segments of length L. For a random level sequence with the Poisson nearest level spacing distribution, the deviation grows linearly, $\Delta(L) = L/15$. For the chaotic case and the Wigner distribution (8), the spectra are rigid. Starting at small L with the same linear behavior, the deviation grows logarithmically at $L \gg 1$,

$$\Delta(L) \approx \frac{1}{\pi^2} \ln L - 0.007. \tag{10}$$

In the semiclassical limit [57], $\Delta(L)$ is expected to saturate at a nonuniversal value of $L \simeq L_{max} \simeq 2\pi\hbar/t_{min}D$ determined by the shortest periodic orbits with a period t_{min}. The number L_{max} measures the Weisskopf recurrence time of a wave packet, $2\pi\hbar/D$, in natural units of the shortest period. At $L > L_{max}$ one expects pseudooscillatory behavior with constant $\Delta(L)$.

Using our 2^+0 states we trace the behavior of $\Delta(L)$ up to very large L. The results, Fig. 5, display an agreement with the GOE prediction with no evidence of saturation up to $L \simeq 150$. At higher L, the spectral rigidity decreases revealing the upbend from the GOE curve. Such behavior is known in "one-body chaos" (anisotropic Kepler problem [58], Sinai billiard [59] or the experiment with a superconducting stadium billiard [60]) where the deviations start at much smaller L. According to Mottelson's conjecture [61], the remnants of regular

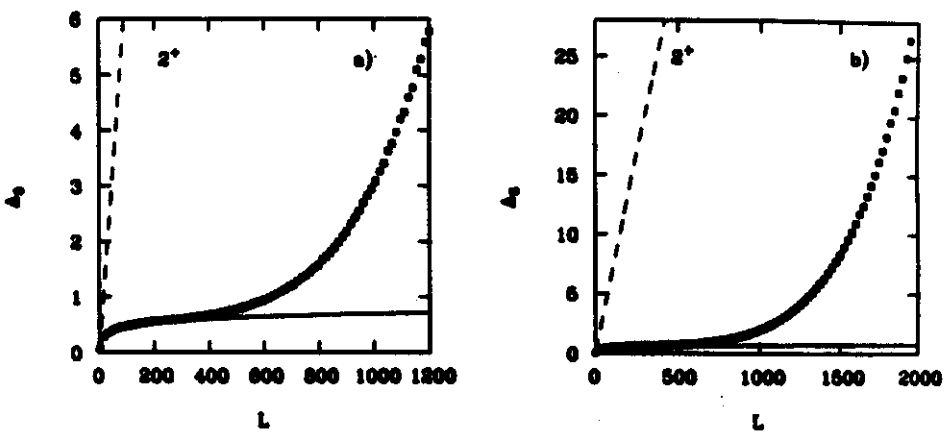

Figure 5: The spectral rigidity $\Delta(L)$ for the 2^+0 states in the limit of large L, $L \leq 1200$ (panel a) and $L \leq 2000$ (panel b); squares (calculations), dashed line (Poisson statistics) and solid line (the GOE prediction).

behavior determine dynamics at times too short to resolve the signatures of chaos. For the stadium billiard [60] the effect is due to the marginally stable "bouncing ball" orbits. In [59] the upbend point L_d was associated with the inverse Lyapunov exponents which give the time scale for the development of classical chaos. The upbend of the curve $\Delta(L)$ starting at $L \approx 200$ corresponds to the energy interval $\delta\epsilon \simeq 7$ MeV. This behavior lasts up to the highest values of $L \approx 2000$ attainable for our computations.

An additional analysis has to be performed to pin down the factors responsible for the upbend. In many-body dynamics within one major shell, the available regular energy parameters are the single-particle level spacings $\delta e \simeq 3$ to 7 MeV which would give $L_d \simeq 100$ to 200. One could also think of the "scars" related to quasiperiodic motion induced by the coherent two-body matrix elements as pairing. In this case one would expect the saturation of $\Delta(L)$ at $L_d \simeq 100$ to 150. The inverse lifetime of the simple configurations can be estimated by the fragmentation width (3), $\bar{\sigma} \simeq 10$ MeV. One can argue that at times shorter than $t_d \simeq 1/\bar{\sigma}$ the chaotic component of the evolution is still of minor importance. It would lead to the upbend of the spectral rigidity at $L_d \simeq \bar{\sigma}/\sqrt{2}D \simeq 200$ which approximately agrees with the observation. However, the time interval t_d cannot in general be identified with the inverse Lyapunov exponent. In contrast to the exponential decay, the survival amplitude decreases as a Gaussian function. The decrease takes place even in the

case of regular dynamics if the initial state is not an eigenstate of the hamiltonian. Another plausible explanation can be associated with the range of the interaction between the simple configurations. We measured this range by the parameter ω_k, eq.(4), which determines the effective band width ~ 7.5 MeV and the corresponding value of L_d between 200 and 250. At shorter time intervals, the band boundaries are not resolved so that motion in the configuration space is analogous to that in the full GOE matrix.

Important information on the stochastization process can be obtained from the level and wave function dynamics as a function of external parameters [8,62]. Apparently, decorrelation of observables under the change of parameters obeys, in the stochastic regime, universal laws where only the scale factors are specific for a given system [63]. The strength λ of the residual interaction can be taken as a natural control parameter in many-body dynamics. The curvature distribution of unfolded energy levels $\mathcal{E}_\alpha(\lambda)$ in the *sd*-shell model takes the GOE form [64,65] at $\lambda \approx 0.3$, in parallel to the level spacing distribution [12].

4 Complexity of wave functions

In the random matrix ensembles, amplitudes C_k^α of eigenstates (5) become random variables. Distribution functions for these amplitudes are known for canonical Gaussian ensembles [66,3]. The GOE case corresponds to complete delocalization when all N components C_k^α for various k contribute equiprobably to the total normalization, and all N eigenfunctions $|\alpha\rangle$ have the same distribution of components. We are interested in the limit $N \gg 1$ when the individual amplitudes are normally distributed with $\bar{C} = 0$ and $\overline{C^2} = 1/N$. The amplitudes in the GOE are slightly correlated [66,3] due to the orthonormalization. Thus, in the limit $N \gg 1$

$$\overline{W_k^\alpha W_l^\beta} = \frac{1}{N^2}(1 + 2\delta^{\alpha\beta}\delta_{kl}), \tag{11}$$

In a gradual transition from regular to stochastic dynamics, the number N_α of principal components of the stationary state $|\alpha\rangle$ increases along with excitation energy towards the limit of complete delocalization. In a given energy range, $E \approx E_\alpha$, the distribution of components C_k^α presumably is similar to the Gaussian but with the local width $\overline{(C_k^\alpha)^2} = 1/N_\alpha$.

Information entropy [67,68,7,69] is a suitable candidate for measuring the degree of complexity of individual wave functions. It is defined for a given normalized function $|\alpha\rangle$, expanded as in eq.(2) with the aid of a given basis

$|k\rangle$, in terms of the weights of the components,

$$S^\alpha = -\sum_k W_k^\alpha \ln W_k^\alpha. \tag{12}$$

Being dependent on the choice of the reference basis $|k\rangle$, this quantity reflects a complicated relationship between the eigenbasis and the basis of representation. The entropy of eigenstates in their own eigenbasis, $W_k^\alpha \to \delta_k^\alpha$, vanishes. The formal maximum of the functional (12) corresponds to the equiprobable distribution, $W_k^\alpha = \text{const} = N^{-1}$, when $S^\alpha = \ln N$. In the local Gaussian approximation, the weights fluctuate around $(N_\alpha)^{-1}$ which implies[7] that the average over the ensemble value of entropy is smaller,

$$\overline{S^\alpha} = \ln(0.48 N_\alpha) + \mathcal{O}(1/N_\alpha). \tag{13}$$

The entropy S^α (12), or the corresponding length in Hilbert space, $l_S^\alpha = \exp S^\alpha$, characterizes the degree of delocalization of a given eigenfunction $|\alpha\rangle$ with respect to the original basis. The deviation of l_S^α from the GOE limit $0.48N$ indicates the incomplete mixing of basis states. For a similar purpose one can use[68] the moments of the distribution of amplitudes,

$$M_n^\alpha = \sum_k (W_k^\alpha)^n, \tag{14}$$

which are also related to the number of principal components of a given eigenstate. The second moment (participation index) M_2^α determines the average $\overline{W^2}$; for the Gaussian average $M_2^\alpha = 3/N^\alpha$. The entropy (12) (or l_S^α) emphasizes the small components of the eigenfunctions, whereas the higher moments (14) emphasize the larger components.

Fig. 6 shows the calculated information lengths l_S^α for all 3276 states 2^+0. We see the strong correlation between information entropy and conventional thermodynamic entropy $\sim \ln \rho$ defined by the level density, Fig. 3. In the most chaotic (middle) part of the spectrum the information entropy reaches about 90% of the GOE value (13). The regular behavior of information entropy allows one to consider this quantity as a function of the excitation energy and, therefore, as a thermodynamic variable. However, if one goes to the case of degenerate single-particle orbitals, the chaotic limit is reached for a significant portion of 0^+0 and 2^+0 states. In this case information entropy ceases to be sensitive to the spectral evolution.

Information entropy behaves similarly in different isospin sectors. In Fig. 7 it is presented for the 0^+0 states of ^{24}Mg in the $p-n$ formalism. Here the GOE value of the entropy is 560. Regardless of the computational procedure,

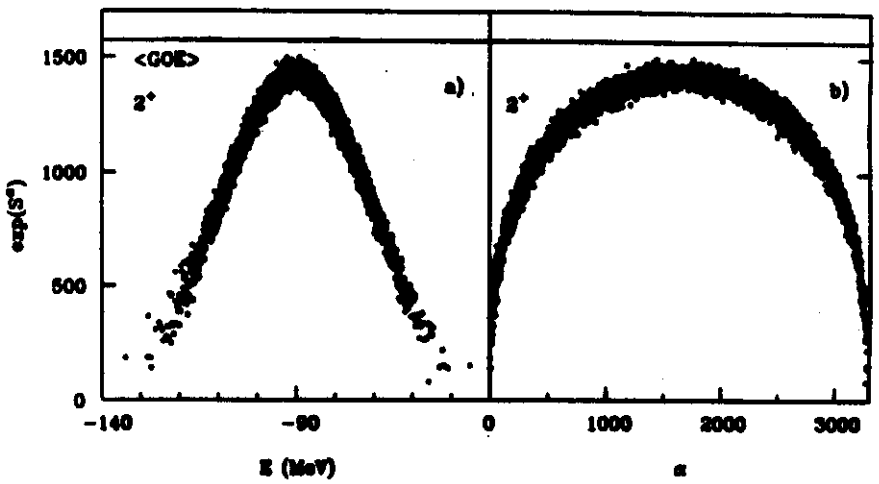

Figure 6: Information length of the 2^+0 states as a function of energy, part *a*, and in the α-scale, part *b*. The horizontal solid line corresponds to the GOE value 1578.

the eigenstates have a certain isospin. However, their information entropies are calculated in the $p-n$ basis where the basis states are mixed in isospin. Therefore the GOE limit refers to the total dimension of $N = 1161$ rather than to the partial dimensions of the 0^+T classes. The families of the states belonging to different isobaric classes can be distinguished by the sequences starting at the corresponding threshold energies.

The overall suppression by a factor λ of the interaction strength changes the results drastically. As we saw, the onset of chaos in the local level statistics occurred at a relatively weak interaction strength. The information entropy of the 0^+0 states at $\lambda = 0.4$ evolves regularly as a function of energy but the localization length is strongly diminished roughly in proportionality to λ.

The behavior of information entropy found in the above example is generic. The calculations were also performed for $N = 1183$ 0^+0 states in ^{12}C in a model space of the first four oscillator shells, taking into account $(0+2)\hbar\omega$ excitations, with the interaction [70] which contains a cross-shell part. In Fig. 8 we can clearly differentiate the states with the lowest c.m. energy (first arch) from those with the excited c.m. motion (second arch). They have the same degree of internal complexity.

Two important features of our results are to be stressed. (i) The information entropy was calculated in the original basis for all individual eigenfunctions with no averaging elements. The eigenfunctions, adjacent in energy, could have different structure and localization properties which would lead to

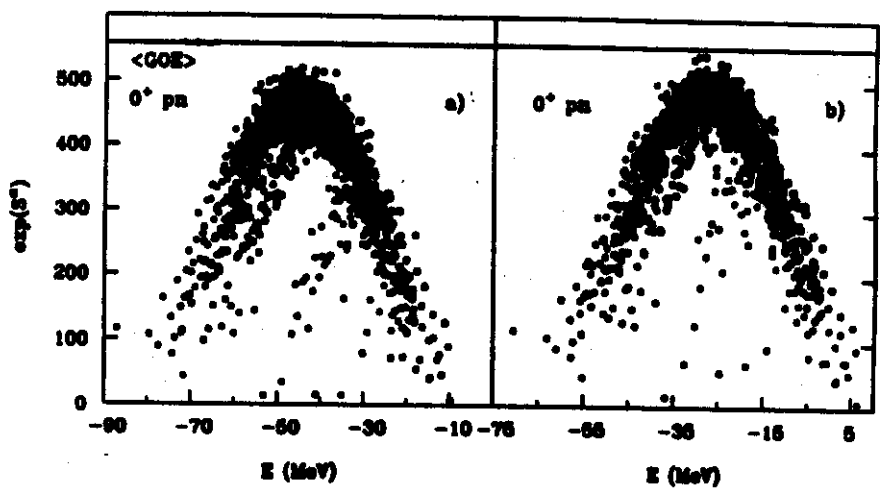

Figure 7: Information length of the 0^+0 states for a system of 4 valence protons and 4 valence neutrons calculated in the $p-n$ formalism with the WPN interaction, part *a*, and the WPNC interaction, part *b*; the solid line corresponds to the GOE value.

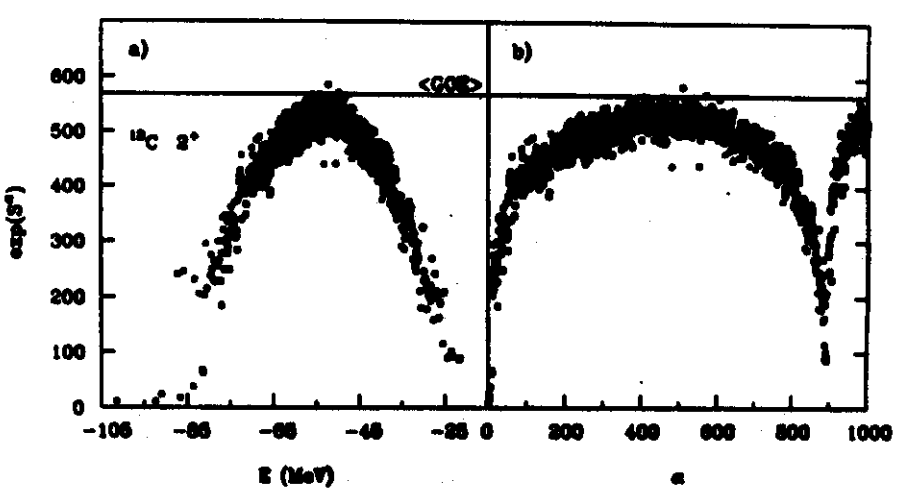

Figure 8: Information length for 1183 2^+0 states in ^{12}C calculated with the Warburton-Brown interaction[70] in 4 major oscillator shell space for $(0+2)\hbar\omega$ excitations; states with and without center-of-mass motion are differentiated in the α-scale. The solid line shows the GOE value.

strong fluctuations. Instead, the degree of complexity regularly evolves along the spectrum reflecting common features of neighboring eigenstates. Being a function of excitation energy only, the degree of complexity can therefore be considered as a thermodynamic variable. (ii) The localization of the eigenfunctions in the shell model basis depends strongly on the strength of the interaction relative to the stabilizing influence of the mean field. This confirms the general trend of the mean field to quench the chaotic signatures of many-body dynamics [69,71].

The results for the "natural" mean field basis can be compared with calculations using different representations. The $SU(3)$ model [72] explains from the group-theoretical viewpoint the appearance of quadrupole deformation and rotational bands. In the basis of the $SU(3)$ eigenfunctions, almost all eigenvectors are completely delocalized. This basis with the degenerate single-particle levels turns out to be almost random with respect to stochastization, analogously to a pure random basis which can also be used as a representation basis for comparison. A certain self-consistency between the representation basis and the residual interaction is necessary to achieve a meaningful description of stochastization. The mean field basis which separates in an optimal way local fluctuations from the global evolution is the most appropriate for this purpose [69].

The use of the moments (14) of the distribution function of the components can give complementary information. The effective number of principal components (NPC) as defined from the participation index, $(NPC)^\alpha = (M_2^\alpha)^{-1}$, is strongly correlated with the level density and the information entropy. It also does not reach the GOE limit $N/3 = 1091$. The deviation is about 12% for the middle part of the spectrum. To see how close is the structure of the eigenfunctions to the random superposition of N_α basis states, one can eliminate the local average value of N_α by calculating various ratios of moments, for example $l_S^\alpha/(NPC)^\alpha$. For a Gaussian distribution, this ratio has the universal value 1.44. The results for the majority of the eigenvectors are close to this expectation.

In the Gaussian BRM ensemble [45] the localization length of eigenstates is proportional to the square of the local level density $\rho(E)$. We found that, except for the edges of the spectrum, the localization length l_S is approximately proportional to $\rho(E)$ rather than to its square. This means the strong correlation between thermodynamic entropy $\sim \ln \rho$ and information entropy.

In the GOE the components of the eigenvectors are dynamically independent. The only source of correlations is the unitarity of the transformation from the original basis $|k\rangle$ to the eigenbasis $|\alpha\rangle$. The correlations of the weights W_k^α, eq. (11), are weak and die out for large N. In contrast to the GOE, the

realistic strongly interacting system has dynamical correlations as pairing built in.

We calculated the correlation functions $N^2\overline{W_k^\alpha W_l^\alpha}$ of different components, $l-k$=1,10,100, and 400. They are close to unity for majority of states in qualitative agreement with the GOE (11) but the short range correlations do still exist. The adjacent components, $l = k+1$, display a pattern almost identical with that for the diagonal case $l = k$, with the same enhancement 1.2 with respect to the GOE. The correlation function for $l = k+10$ is also enhanced by the factor 1.2 in the middle. If the normalization factor in the definition of the correlation function were taken as N_α^2 instead of N^2, in the middle part of the spectrum one would receive $N_\alpha/N = (1.2)^{-1/2} = 0.9$ in agreement with what we extracted from information entropy and the NPC. The long range correlation functions, $l = k+100$ and $l = k+400$, are close to unity with correlational edges strongly suppressed. The correlation length of the order of 100 in the k-scale, or of the order of 10 MeV in the energy scale, agrees with the magnitude of the energy dispersion of eq.(3) which is related to the fragmentation of the basis states and the spreading width. The correlation function of the adjacent components $\overline{W_k^\alpha W_{k+1}^\alpha}$ multiplied by $[\exp(S^\alpha)/0.48]^2$, or by $[3(NPC)^\alpha]^2$, would be equal to unity for the Gaussian distribution with an effective local number of states N_α. These products approach unity in the middle part but they still depend on excitation energy. The effective number of components is smaller than the decorrelation factor in (11), except for the most complicated states. It means that decorrelation occurs faster than the delocalization of the wave functions, and the actual distribution function of the eigenvector components systematically deviates from the local Gaussian.

In using information entropy or other similar measures one needs to distinguish a genuine chaotic behavior from the complexity associated with collective motion or with the improper choice of the basis. Collective excitations $|c\rangle$ also can be presented by superpositions (2). In this case the amplitudes C_k^c are coherent with respect to a certain simple (one-body in the RPA) operator Q. The phases of the amplitudes C_k^c are synchronized with those of the matrix elements Q_{k0} for a transition between simple states, for example the ground state $|0\rangle$ and a $1p-1h$ state $|k\rangle$. The partial amplitudes add constructively so that the transition probability $|0\rangle \to |c\rangle$ is enhanced, as compared to the elementary transition $|0\rangle \to |k\rangle$, by a factor N^c which is a number of coherent components contributing to the wave function $|c\rangle$. If N^c is large, our measures of complexity will signal an appearance of a complicated state which has nothing to do with chaos.

However (i) the fraction of collective states is small ($\sim 1/N^c$), (ii) the degree of collectivization in nuclei N^c is small compared to the degree of com-

plexity of typical complicated states (in heavy nuclei $N^c \simeq 10^2$ for low lying excitations of vibrational or rotational type but $N \simeq 10^6$ for neutron resonances), and (iii) in a realistic many-body system only the lowest collective states are approximately stationary, but in that energy domain there is no chaos anyway. Collective states at higher excitation energy are strongly mixed (damped), so the only surviving signature of collectivity ("scar") could be a nonstatistical excess of specific $1p-1h$ basis components concentrated at a certain energy in the interval of the spreading width and manifested by a peak of the strength function of the operator Q.

The problems associated with an inappropriate choice of the basis can be more dangerous. Considering a tight binding model of a particle in a periodic N-well potential and using the localized states as the basis states, we find for the Bloch wave solutions $(NPC) = (2/3)(N+1)$ for all wave vectors. This complexity, being higher than in the GOE ensemble, is a manifestation of the uncertainty relation between the coordinate and the wave vector. (In our studies we never saw complexity which would considerably exceed the GOE limit). In many cases there exists a smooth evolution or phase transition of the mean field along with increasing energy. Even if the new shape supports regular single-particle motion, this can be misinterpreted as onset of chaos due to the complexity of new eigenstates expressed in the old representation. But in such cases the invariant measures of chaos connected to the level statistics unequivocally indicate absence of chaos. As an example, we studied [12] the pairing correlations as a function of excitation energy. This specific probe allows one to trace the behavior similar to the second order phase transition through the properties of individual eigenfunctions.

5 Chaoticity *vs* thermalization

We saw that the stationary states display the conventional signatures of quantum chaoticity. Local level correlations reveal Wigner repulsion. The spectra are rigid with no pronounced contribution from periodic orbits. The partition structure is smeared, the eigenstates are delocalized and their information entropy (12) in the shell-model basis is close to the GOE limit. These signatures give clear evidence that our system, at least in the middle of the energy range, is near the stochastic limit. Along with this, there exists a noticeable change of complexity as a function of excitation energy. The thermodynamic picture is frequently used in the description of excited states at high level density. What is the relation between the complicated structure of eigenstates and statistical mechanics? To address this question we first discuss the notion of statistical equilibrium as applied to an isolated mesoscopic system like a nucleus.

Statistical properties of a closed equilibrated system with a sufficiently high number of degrees of freedom are determined by the statistical weight $\Omega(E) = \rho(E)\delta E$ of states with given values of exact integrals of motion. Since the density of states $\rho(E)$ grows fast with energy E, the interval δE can still contain many levels which makes the concept of the smooth level density meaningful. The exact value of δE is not important as long as it is small compared to the energy interval where the macroscopic properties of the system change considerably. Now one can define thermodynamic entropy $S^{th}(E) = \ln \Omega(E)$ and temperature T according to

$$\frac{\partial S^{th}}{\partial E} = \frac{1}{T}. \tag{15}$$

Such a description corresponds to the minimum information available. Our knowledge of the microscopic state of the system at equilibrium is limited to what is given by exact integrals of motion.

The accuracy of the statistical approach implies that the results are insensitive to the actual microscopic state of the system. Average over the equilibrium statistical ensemble should give the same outcome as an expectation value for a typical stationary wave function at the same energy [73]. The main underlying assumption is that of similarity of generic wave functions in a given energy region. At the same time, equilibrium statistical averaging discards possible phase relationships between the components of wave functions. This is justified if the phase coherence can appear with a very low statistical weight only. The similarity of close eigenstates is ensured by the mixing resulting from the chaotic many-body dynamics. The pioneering paper on the compound nucleus by Niels Bohr [16] already gives an equal footing to elements of both patterns, chaos and thermalization. The definition by Percival [74] of chaotic wave functions goes along the same line. It was shown by van Hove [75] that a broad class of systems displays quantum ergodicity: a random initial wave function evolves with time into a state which gives the same values of observables as the microcanonical thermodynamic ensemble, see also [76].

We can compare statistical properties of eigenfunctions of the Fermi system with strong interaction (although in a truncated space) with those of the equilibrium statistical ensemble. The degree of complexity measured by information entropy of individual functions in the shell-model basis is the same for many states close in energy. Within small fluctuations, it changes smoothly with excitation energy and can be treated as a thermodynamic variable. To compare the global thermodynamic behavior with the features of the individual eigenfunctions, we calculate the evolution of single-particle occupation

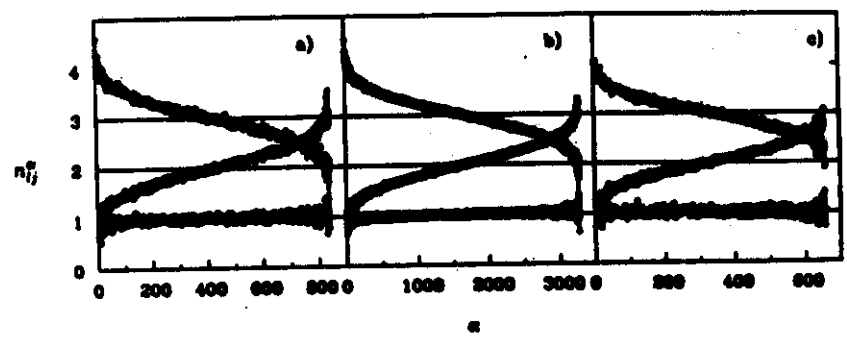

Figure 9: Single-particle occupation numbers for states 0^+0 (panel a), 2^+0 (panel *b*), and 9^+0 (panel *c*). For all panels the three sets of points refer to $s_{1/2}, d_{3/2}$ and $d_{5/2}$ orbitals, from bottom to top on the left-hand side.

numbers n^{α}_{lj} along the spectrum of many-body states $|\alpha\rangle$,

$$n^{\alpha}_{lj} = \frac{1}{2}\sum_{m\tau}\langle\alpha|a^{\dagger}_{ljm\tau}a_{ljm\tau}|\alpha\rangle. \tag{16}$$

The results are shown in Fig. 9 where the panels a,*b* and *c* correspond to 0^+0, 2^+0 and 9^+0 $(N = 657)$ states, respectively. All three classes of states exhibit an identical smooth behavior. It suggests that one can associate with each eigenstate $|\alpha\rangle$ a single-particle "temperature" T^{α}_{s-p} defined by the Fermi distribution

$$f^{\alpha}_{lj} = \{\exp[(e'_{lj} - \mu)/T^{\alpha}_{s-p}] + 1\}^{-1}. \tag{17}$$

In the center (infinite temperature), all occupancies $f^{\alpha}_{lj} = n^{\alpha}_{lj}/(2j+1)$ indeed become equal to each other the common value being 1/2 for our case of 12 particles in the *sd*-shell of the total capacity 24.

T^{α}_{s-p} changes smoothly with energy, being almost the same for all states within the narrow energy interval as it should be for an intensive thermodynamic quantity. It becomes infinite simultaneously with the thermodynamic temperature when the memory of the initial single-particle energies is lost. The effective energies $e'_{lj} - \mu$ can be found [11,12] from the fit or directly from the slopes of the lines in Fig. 9; they are close to the bare values. Using these energies, one can extract the effective temperature T^{α}_{s-p} and check that, despite

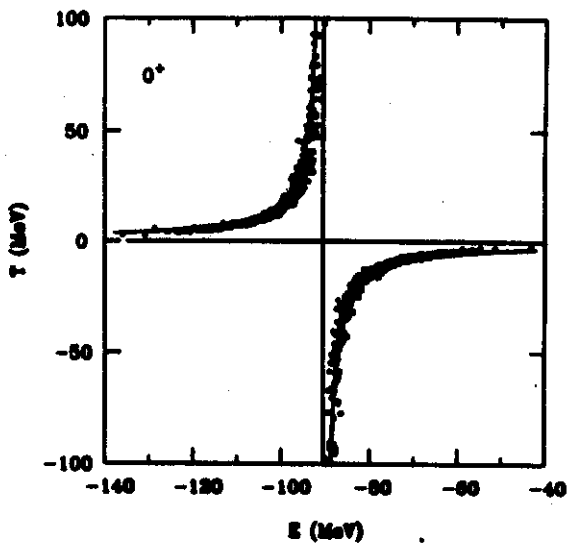

Figure 10: Temperature calculated from the global fit to the level density of the 0^+0 states (solid line) and found from the occupation numbers of Fig. 9 (dots).

the strong interaction, the "single-particle thermometer" on average measures the same temperature as T obtained from the level density. For the Gaussian level density $\rho(E)$ with the centroid at E_0 and variance σ_E^2, the temperature (15), see Fig. 10 (solid lines), is

$$T = \sigma_E^2/(E_0 - E). \tag{18}$$

The right half of the spectrum, $E > E_0$, is associated with decreasing entropy and negative temperature.

These results imply that the system can be considered as an equilibrated Fermi-liquid, and its properties can be expressed in terms of occupation numbers for a gas of interacting quasiparticles. We do not perform any ensemble averaging. The eigenfunctions individually show the distribution of occupancies expected from statistical mechanics of the equilibrium thermal ensemble. Thermodynamics of the system are determined mainly by the stabilizing action of the mean field. Using the mean field basis we segregate the incoherent processes leading to stochastization and chaos from the regular evolution along the spectrum. The stochastic part of the dynamics is responsible for the complexity of the eigenfunctions and their similarity, which can be interpreted in terms of thermal equilibrium. The regular (mean field) features allow us to use a simple language of average occupation numbers for quasiparticles in a heated Fermi liquid.

We mentioned that a certain level of self-consistency between the mean

field and the residual interaction is necessary for the optimal separation of local and global features. In the shell-model calculations it is ensured by the semiempirical hamiltonian. In this case we can expect a strong correlation between the thermodynamical entropy (lack of knowledge about the precise microscopic state of the system) and information entropy (disorder of a given microscopic state computed in the mean field basis of simple quasiparticle configurations). A direct comparison indeed reveals such a correlation.

Using the occupancies f_{lj}^{α} of individual orbitals one can calculate the single-particle entropy of the quasiparticle gas [73] for each state $|\alpha\rangle$,

$$S_{s-p}^{\alpha} = -\sum_{lj\tau}(2j+1)[f_{lj}^{\alpha}\ln f_{lj}^{\alpha} + (1-f_{lj}^{\alpha})\ln(1-f_{lj}^{\alpha})]. \qquad (19)$$

The expression (19) comes from the Fermi-gas combinatorics. Now we have three, apparently different, entropy-like quantities: thermodynamic entropy $S^{th}(E) \sim \ln\rho(E)$, information entropy S^{α} (12) and single-particle entropy S_{s-p}^{α} (19), the latter two for individual eigenstates.

For a weak off-diagonal interaction [11,12], the thermodynamic entropy displays Gaussian behavior of a combinatorial nature typical for an imperfect Fermi-gas in a finite number of states. Within the fluctuations, it is quite similar to the single-particle entropy. The information entropy in this case is low; only at high level density does one see some effects of mixing. This is an equilibrium picture of almost non-interacting particles where the degree of complexity given by the information entropy is only weakly correlated with thermalization. Using the language of kinetic theory, collisions (mixing) are necessary for equilibration but the equilibrium properties do not depend on the collision rate.

In the opposite case of too strong off-diagonal interaction, all states are strongly mixed and the information entropy is near the GOE maximum. The memory of the mean field is lost and S_{s-p}^{α} is also at the maximum corresponding to the equiprobable population of orbitals so that the response to thermal excitation cannot be expressed in terms of quasiparticles. Within the fluctuations, S^{α} and S_{s-p}^{α} coincide. The interaction is too strong, almost all wave functions "look the same" regardless of level density, and the quasiparticle "thermometer" cannot resolve the spectral regions with different temperatures. However, the system still has normal thermodynamic properties governed by the level density. In this case only the microcanonical description is possible.

For the realistic mean field and self-consistent residual interaction, all three entropies (correspondingly normalized) turn out [11] to be identical within fluctuations except for the edges of the spectrum. Near the ground state the Fermi surface is already smeared due to two-body correlations so that the

single-particle occupation numbers and information entropy show deviations from the frozen Fermi-gas. The difference between low thermodynamic temperature and single-particle temperature, as measured for instance in particle knockout experiments near the ground state, was discussed in [69]. For the majority of states and for the mean field consistent with residual interactions, the thermodynamic entropy (defined either via the global level density or in terms of occupation numbers) behaves similarly to information entropy.

6 Conclusions

The nuclear shell model provides a realistic, exactly solvable example of a many-fermion system with strong interaction. The available dimensions are sufficiently high to allow for statistically reliable studies. The construction of the complete set of states with the given values of exact integrals of motion is an important prelude to the analysis. The role of this premixing and "geometrical chaoticity" is to be further studied. The exponential distribution of the off-diagonal matrix elements of the residual interaction appears a generic feature of the realistic many-body systems.

As excitation energy and level density increase, the local level statistics quickly reveal signatures of chaotic dynamics predicted by the GOE. This occurs for an interaction strength much lower than its actual value. The problem of the transitional nearest-level spacing distribution in the region of onset of chaos and the fractional power law for level repulsion remains to be solved.

The degree of complexity of stationary wave functions can be measured by the information entropy and the moments of the distribution function of the components. These measures depend on the representation which can be used to gain additional knowledge on the structure of the eigenvectors. The mean field (shell-model) basis appears to be the preferred representation which allows for the optimal separation of local spectral properties from global secular dynamics. The structure of the wave functions presented in the mean field basis evolves in a regular way along the spectrum. The measures of complexity can be considered as functions of the excitation energy. The distribution of the components of the eigenvectors in the shell model basis is close to Gaussian although the correlational analysis reveals deviations. The GOE limit of the complete delocalization can be reached by the majority of the eigenvectors only with an artificially suppressed stabilizing action of the mean field.

The single-particle occupation numbers of the shell-model orbitals regularly evolve along the spectrum, being nearly the same for different classes of states. They can be described by the Fermi distribution with effective energies close to the bare ones. The similarity of the wave functions and occupation

numbers of the states close in energy can be interpreted in terms of statistical equilibrium. In spite of the presence of strong interactions, the system behaves at high excitation energy as a heated Fermi gas of fermionic quasiparticles. This indicates the possibility of using the thermal ensemble for calculating matrix elements between the compound states [77]. The apparent decoherence emerges here as a property of individual complicated wave functions in a closed mesoscopic system, with no heat bath involved. Different definitions of temperature, related to the thermal microcanonical ensemble, single-particle occupancies, and information entropy, practically coincide for the mean field representation used in the last two cases, where the temperature scale is extracted for each individual eigenstate. It gives new arguments for understanding the foundations of quantum statistical mechanics and its relationship to quantum chaos.

Acknowledgments

The authors acknowledge support from the NSF grant 94-03666.

1. *Statistical Theories of Spectra: Fluctuations*, ed. C.E. Porter (Academic Press, New York, 1965).
2. A.Bohr and B.Mottelson, *Nuclear Structure*, vol. 1 (Benjamin, New York, 1969).
3. T.A.Brody, J.Flores, J.B.French, P.A.Mello, A.Pandey and S.S.M.Wong, Rev. Mod. Phys. **53**, 385 (1981).
4. P.V.Elyutin, Usp. Fiz. Nauk **155**, 397 (1988) [Sov. Phys. Usp. **31**, 597 (1988)].
5. O.Bohigas and H.A.Weidenmüller, Ann. Rev. Nucl. Part. Sci. **38**, 421 (1988).
6. H.G.Schuster, *Deterministic Chaos* (VCH Verlagsgesellschaft, Weinheim, 1989).
7. F.M.Izrailev, Phys. Rep. **196**, 299 (1990).
8. F.Haake, *Quantum Signatures of Chaos* (Springer, New York, 1991).
9. V.G.Zelevinsky, Nucl. Phys. **A553**, 125c (1993); **A570**, 411c (1994).
10. V.Zelevinsky, M.Horoi and B.A.Brown, Phys. Lett. **B350**, 141 (1995).
11. M.Horoi, V.Zelevinsky and B.A.Brown, Phys. Rev. Lett. **74**, 5194 (1995).
12. V.Zelevinsky, B.A.Brown, N.Frazier and M.Horoi. Phys. Reports, *in press.*
13. G.E.Mitchell *et al.*, Phys. Rev. Lett. **61**, 1473 (1988); J.F.Shriner, Jr. *et al.*, Z. Phys. **A335**, 393 (1990).

14. S.Raman *et al.*, Phys. Rev. **C43**, 521 (1991).
15. J.D.Garrett *et al.*, *Future Directions with 4π Gamma Detection Systems of the New Generation*, ed. J.Dudek and B.Haas (AIP, 1991) p.345.
16. N.Bohr, Nature **137**, 344 (1936).
17. O.P.Sushkov and V.V.Flambaum, Pis'ma Zh. Exptl. Teor. Fiz. **32**, 377 (1980) [JETP Lett. **32**, 353 (1980)]; Usp. Fiz. Nauk **136**, 3 (1982) [Sov. Phys. Usp. **25**, 1 (1982)].
18. V.V.Flambaum and G.F.Gribakin, Prog. Part. Nucl. Phys., **35**, 423 (1995).
19. H.L.Harney, A.Richter and H.A.Weidenmüller, Rev. Mod. Phys. **58**, 607 (1986).
20. V.G.Zelevinsky and P. von Brentano, Nucl. Phys. **A529**, 141 (1991).
21. J.J.Gaardhøje, Annu. Rev. Nucl. Part. Sci. **42**, 483 (1992).
22. B.Lauritzen, P.F.Bortignon, R.A.Broglia and V.G.Zelevinsky, Phys. Rev. Lett. **74**, 5190 (1995).
23. C.A.Bertulani and V.G.Zelevinsky, Nucl. Phys. **A568**, 931 (1994).
24. C.H.Lewenkopf and V.G.Zelevinsky, Nucl. Phys. **A569**, 183 (1994).
25. B.Lauritzen, T.Døssing and R.A.Broglia, Nucl. Phys. **A457**, 61 (1986).
26. M.Matsuo *et al.*, Nucl. Phys. **A557**, 211c (1993); T.Døssing *et al.*, Phys. Rep., *in press*.
27. B.A.Brown and B.H.Wildenthal, Ann. Rev. Nucl. Part. Sci. **38**, 29 (1988).
28. B.A.Brown, A.Etchegoyen, W.D.M.Rae, W.E.Ormand, J.S. Winfield and L.Zhao, *OXBASH code*, MSUNSCL Report **524**, (1988).
29. B.A.Brown and G.Bertsch, Phys. Lett. **148B**, 5 (1984).
30. W.E.Ormand and R.A.Broglia, Phys. Rev. **C46**, 1710 (1992).
31. N.Auerbach and B.A.Brown, Phys. Lett. **B340**, 6 (1994).
32. V.Lopac, S.Brant and V.Paar, Z. Phys. **A337**, 131 (1990).
33. Y.Alhassid and A.Novoselsky, Phys. Rev. **C45**, 1677 (1992).
34. D.C.Meredith, S.E.Koonin, and M.R.Zirnbauer, Phys. Rev. **A37**, 3499 (1988).
35. V.V.Flambaum, G.F.Gribakin and F.M.Izrailev, *to be published.*
36. V.V.Flambaum, A.A.Gribakina, G.F.Gribakin and M.G.Kozlov, Phys. Rev. **A50**, 267 (1994).
37. J.Brenneisen et al., Z. Phys. **A352**, 149, 279, 403 (1995).
38. W.E.Ormand and B.A.Brown, Nucl. Phys. **A491**, 1 (1989).
39. J.B.French and K.F.Ratcliff, Phys. Rev. **C3**, 94 (1971); K.F.Ratcliff, Phys. Rev. **C3**, 117 (1971).
40. N.Frazier, B.A.Brown and V.Zelevinsky, *to be published.*
41. M.Horoi, B.A.Brown and V.Zelevinsky, Phys. Rev. **C50**, R2274 (1994).

42. M.Feingold, D.M.Leitner and M.Wilkinson, Phys. Rev. Lett. **66**, 986 (1991).
43. E.P.Wigner, Ann. Math. **62**, 548 (1955).
44. J.Casati *et al.*, Phys. Rev. Lett.**64**, 1 (1990); M.Kuś, M.Lewenstein and F.Haake, Phys. Rev. **A44**, 2800 (1991).
45. Y.V.Fyodorov and A.D.Mirlin, Phys. Rev. Lett. **67**, 2405 (1991).
46. J.Wambach, private communication.
47. D.Kusnezov, private communication.
48. J.B.French and S.S.M.Wong, Phys. Lett. **B35**, 5 (1971); K.K.Mon and J.B.French, Ann. Phys. **95**. 90 (1975).
49. I.I.Gurevich and M.I.Pevsner, Nucl. Phys. **2**, 575 (1957).
50. M.Berry and M.Robnik, J. Phys. **A17**, 2413 (1984); M.Berry, Proc. Roy. Soc. **A400**, 229 (1985).
51. V.V.Sokolov and V.G.Zelevinsky, Phys. Lett. **B202**, 10 (1988); Nucl. Phys. **A504**, 562 (1989); Ann. Phys. **216**, 323 (1992).
52. S.Mizutori and V.G.Zelevinsky, Z. Phys. **A346**, 1 (1993).
53. T.Prosen and M.Robnik, J. Phys. **A26**, 2371 (1993).
54. L.Molinari and V.V.Sokolov, J. Phys. **A22**, L999 (1989).
55. A.Altland and D.Fuchs, Phys. Rev. Lett. **74**, 4269 (1995).
56. O.Bohigas, M.J.Giannoni and C.Schmit, Phys. Rev. Lett. **52**, 1 (1984).
57. M.V.Berry, Proc. Roy. Soc. London, Ser. A **400**, 229 (1985).
58. D.Wintgen and H.Marxer, Phys. Rev. Lett. **60**, 971 (1988).
59. P.Arve, Phys. Rev. **A44**, 6920 (1991).
60. H.-D.Gräf, H.L.Harney, H.Lengeler, C.H.Lewenkopf, C.Rangacharyulu, A.Richter, P.Schardt and H.A.Weidenmüller, Phys. Rev. Lett. **69**, 1296 (1992).
61. B.Mottelson, *unpublished.*
62. A.Szafer and B.L.Altshuler, Phys. Rev. Lett. **70**, 587 (1993).
63. D.Kusnezov and C.H.Lewenkopf, *in press*; D.Kusnezov, B.A.Brown and V.Zelevinsky, *to be published.*
64. J.Zakrzewski and D.Delande, Phys. Rev. **E47**, 1650 (1993).
65. F. von Oppen, Phys. Rev. Lett. **73**, 798 (1994).
66. N.Ullah and C.E.Porter, Phys. Lett. **6**, 301 (1963); N.Ullah, *Int. Nucl. Phys. Conf.*, ed. R.L.Becker (Academic, New York, 1967) p. 812.
67. F.J.Yonezawa, Non-Cryst. Solids **35 & 36**, 29 (1980).
68. J.Reichl, Europhys. Lett. **6**, 669 (1988).
69. V.G.Zelevinsky, Nucl. Phys. **A555**, 109 (1993).
70. E.K.Warburton and B.A.Brown, Phys. Rev. **C46**, 923 (1992).
71. W.Bauer, D.McGrew, V.Zelevinsky and P.Schuck, Phys. Rev. Lett. **72**, 3771 (1994); Nucl. Phys. **A583**, 93 (1995).

72. J.P.Elliott, Proc. Roy. Soc. **A245**, 128, 562 (1958).
73. L.D.Landau and E.M.Lifshitz, *Statistical Physics* (Pergamon Press, 1958).
74. I.C.Percival, J. Phys. **B6**, L229 (1973).
75. L. van Hove, Physica **21**, 517 (1955); **23**, 441 (1957); **25**, 268 (1959).
76. M.Srednicki, Phys. Rev. **E50**, 888 (1994).
77. V.V.Flambaum and O.K.Vorov, Phys. Rev. Lett. **70**, 4051 (1993).